AGU ADVANCING EARTH AND SPACE SCIENCES

Geophysical Research Letters®

RESEARCH LETTER
10.1029/2023GL104139

Saturation of Ocean Surface Wave Slopes Observed During Hurricanes

Jacob R. Davis[1], Jim Thomson[1], Isabel A. Houghton[2], James D. Doyle[3], William A. Komaromi[4], Chris W. Fairall[5], Elizabeth J. Thompson[5], and Jonathan R. Moskaitis[3]

[1]Applied Physics Laboratory, University of Washington, Seattle, WA, USA, [2]Sofar Ocean, San Francisco, CA, USA, [3]Naval Research Laboratory, Monterey, CA, USA, [4]I.M. Systems Group, Inc., NOAA/NWS/OSTI, Silver Spring, MD, USA, [5]NOAA Physical Sciences Laboratory (PSL), Boulder, CO, USA

Key Points:

- Buoy observations of waves in hurricanes show the dependence of wave slope on wind speed changes above 15 m s^{-1} and saturates beyond 30 m s^{-1}
- Wave spectra become dominated by the saturation range at high winds suggesting wave breaking is ubiquitous and thereby limits wave slope
- This effect is a plausible cause for the reduction of surface drag at high wind speeds

Supporting Information:

Supporting Information may be found in the online version of this article.

Correspondence to:

J. R. Davis,
davisjr@uw.edu

Citation:

Davis, J. R., Thomson, J., Houghton, I. A., Doyle, J. D., Komaromi, W. A., Fairall, C. W., et al. (2023). Saturation of ocean surface wave slopes observed during hurricanes. *Geophysical Research Letters*, *50*, e2023GL104139. https://doi.org/10.1029/2023GL104139

Received 17 APR 2023
Accepted 26 JUL 2023

Author Contributions:

Conceptualization: Jacob R. Davis, Jim Thomson, Isabel A. Houghton, Chris W. Fairall, Elizabeth J. Thompson
Data curation: Jacob R. Davis, Isabel A. Houghton, James D. Doyle, William A. Komaromi, Jonathan R. Moskaitis
Formal analysis: Jacob R. Davis, Jim Thomson, Isabel A. Houghton, Chris W. Fairall

Abstract Drifting buoy observations of ocean surface waves in hurricanes are combined with modeled surface wind speeds. The observations include targeted aerial deployments into Hurricane Ian (2022) and opportunistic measurements from the Sofar Ocean Spotter global network in Hurricane Fiona (2022). Analysis focuses on the slope of the waves, as quantified by the spectral mean square slope. At low-to-moderate wind speeds (<15 m s^{-1}), slopes increase linearly with wind speed. At higher winds (>15 m s^{-1}), slopes continue to increase, but at a reduced rate. At extreme winds (>30 m s^{-1}), slopes asymptote. The mean square slopes are directly related to the wave spectral shapes, which over the resolved frequency range (0.03–0.5 Hz) are characterized by an equilibrium tail (f^{-4}) at moderate winds and a saturation tail (f^{-5}) at higher winds. The asymptotic behavior of wave slope as a function of wind speed could contribute to the reduction of surface drag at high wind speeds.

Plain Language Summary Drifting buoy observations of ocean surface waves in Hurricanes Ian and Fiona (2022) are combined with modeled wind speed to explore the evolution of the sea surface from moderate to extreme winds (up to 54 m s^{-1}). The sea surface is characterized using the physical slope of the waves, or the ratio of a wave's height to its length, which has previously only been well-understood up to moderate wind speeds of 15–20 m s^{-1}. At lower wind speeds, the average slopes increase proportional to the wind speed, meaning the waves continually steepen as the wind strengthens. At higher winds, the slopes continue to increase, but at a reduced rate. The slopes eventually reach a maximum value at the most extreme winds (i.e., the slopes saturate). This phenomenon is accompanied by a change in sea surface character from one that is patterned by occasional wave breaking to one that is almost entirely covered by whitecaps and foam. Using wave slope as a measure of the roughness of the ocean surface, the observed wave slope saturation could help to explain the relative reduction in wind surface forcing at extreme wind speeds.

1. Introduction

The physical slope of ocean surface waves, defined as the ratio of a wave's height to its length (H/L) or product of its amplitude and wavenumber (ak), is widely found to play a governing role in the exchange of momentum at the air-sea interface. Slope is essential in the parameterization of deep-water breaking processes (Drazen et al., 2008; Duncan, 1981; Melville, 1994; Schwendeman & Thomson, 2017; Schwendeman et al., 2014, and others) and is theorized to contribute to the air-sea drag coefficient through modulation of the aerodynamic roughness (Donelan, 2018; Lan et al., 2022; Takagaki et al., 2012, 2016; Taylor & Yelland, 2001; Troitskaya et al., 2012). Efforts to characterize slope as a function of wind speed trace back to Cox and Munk (1954), who used optical measurements of the sun's glint to measure the distribution of slopes in wind speeds ranging from 1 to 14 m s^{-1}. This work was followed by an extensive set of satellite radiometer measurements reported by Bréon and Henriot (2006) up to 12 m s^{-1}, the airborne lidar-based measurements of Lenain et al. (2019) from 2 to 13 m s^{-1}, and most recently, the spaceborne measurements of Guérin et al. (2022) and Li et al. (2022). These works universally agree that, in low-to-moderate winds, the mean square of the slope distribution, or *mean square slope*, increases linearly with wind speed. Dynamics above 20 m s^{-1} remain less thoroughly investigated.

The mean square slope (mss) is a metric that quantifies the average steepness of waves over a range of frequencies or wavenumbers. When estimated from the wave energy density spectrum (sea surface elevation variance spectrum), it is an integral quantity proportional to the fourth moment of the spectrum. It can be calculated across any

Funding acquisition: Jim Thomson, Isabel A. Houghton, James D. Doyle, William A. Komaromi, Chris W. Fairall, Elizabeth J. Thompson, Jonathan R. Moskaitis
Investigation: Jacob R. Davis, Jim Thomson, Isabel A. Houghton
Methodology: Jacob R. Davis, Jim Thomson, Isabel A. Houghton, James D. Doyle, William A. Komaromi, Jonathan R. Moskaitis
Project Administration: Jim Thomson, Isabel A. Houghton, Chris W. Fairall, Elizabeth J. Thompson
Resources: Jacob R. Davis, Jim Thomson, Isabel A. Houghton, James D. Doyle, William A. Komaromi, Jonathan R. Moskaitis
Software: Jacob R. Davis, Isabel A. Houghton, James D. Doyle, William A. Komaromi, Jonathan R. Moskaitis
Supervision: Jim Thomson, Isabel A. Houghton, Chris W. Fairall, Elizabeth J. Thompson
Validation: Jacob R. Davis, Jim Thomson, Isabel A. Houghton, Chris W. Fairall, Elizabeth J. Thompson
Visualization: Jacob R. Davis, Jim Thomson
Writing – original draft: Jacob R. Davis, Jim Thomson
Writing – review & editing: Jacob R. Davis, Jim Thomson, Isabel A. Houghton, James D. Doyle, William A. Komaromi, Chris W. Fairall, Elizabeth J. Thompson, Jonathan R. Moskaitis

portion (or the entirety) of the spectrum, and it is closely related to the shape of the spectrum itself. Typically, the actively forced, wind-driven gravity wave spectra in hurricanes have a single peak followed by a broad spectral "tail" (Young, 2003). The canonical tail of a wind-driven gravity wave spectrum has two distinct regions: an *equilibrium range* and a *saturation range* (Banner, 1990; Forristall, 1981; Lenain & Melville, 2017). The *equilibrium range* is defined by a balance of wind input, dissipation from breaking, and nonlinear energy fluxes. It begins just beyond the peak frequency and is characterized by a distinct f^{-4} spectral slope in frequency, or $k^{-5/2}$ in wavenumber space (Phillips, 1985; Toba, 1973). At frequencies beyond the equilibrium range, a *saturation range* exists, where the wind input is balanced by dissipation from breaking (Banner, 1990; Forristall, 1981; Lenain & Melville, 2017; Romero et al., 2012). This region is characterized by a spectral slope of f^{-5} (k^{-3} in wavenumber space). In the remaining discussion, the "saturation" range will be referred to as the "dissipation" range to avoid confusion with the use of saturation to describe the wind speed dependence of mss.

Wave slope and spectral shape, particularly the tail, are closely tied to the wind forcing. Through the use of a Phillips (1985) analytical expression for spectral energy in the equilibrium range related to mean square slope, Thomson et al. (2013) demonstrated the feasibility of estimating wind stress based on wave spectral observations alone. In that work, the equilibrium-derived estimates of wind speed compare well with observed wind speeds up to 15 m s^{-1}, enabling operational use of the method to derive proxy wind speeds in the Sofar Spotter global network (Voermans et al., 2020). However, at higher wind speeds, the dependence of mss remains largely unexplored, except in models (Donelan, 2018) and in the laboratory (Takagaki et al., 2012, 2016).

The complex nature of hurricane waves has been studied and reported on for over a century (Cline, 1920) with the first in situ observations emerging around 1970 (e.g., Patterson, 1974; Whalen & Ochi, 1978). Waves evolve rapidly in hurricanes, especially in fast-moving storms under which the "extended" or "effective" fetch (King & Shemdin, 1978) and duration of forcing changes with storm translation speed (Hell et al., 2021; J.-Y. Hsu et al., 2019; Hwang, 2016; Hwang & Fan, 2017; Kudryavtsev et al., 2015). Wave directions vary dramatically based on location relative to the center of the storm, with large wind-wave misalignment possible in the left quadrants (Collins et al., 2018; J.-Y. Hsu, 2021; Hwang & Walsh, 2018; Tamizi & Young, 2020; Walsh et al., 2002; Young, 2006). The interaction of waves and currents can also be significant (Bruciaferri et al., 2021; Hegermiller et al., 2019; Sun et al., 2022; Yujuan et al., 2018). Waves, both breaking and non-breaking, play a substantial role in the exchange of momentum and heat at the air-sea interface (Holthuijsen et al., 2012; S. A. Hsu et al., 2017; Kita & Waseda, 2022). This literature has lacked an observed relation between wave slopes and wind speeds in hurricanes that can be used to improve the modeling of surface stress and wave growth in this extreme environment (Janssen & Bidlot, 2023). These physics are essential for the modeling of tropical cyclone intensity and coastal inundation.

Here, we use buoy spectral measurements in hurricane winds to study the evolution of wave slope and spectral shape as a function of modeled wind speed. Section 2 describes the determination of *mss* from the buoys and describes the coupled model used for surface wind speeds. Section 3 presents the results, and Section 4 discusses the implications and relation to other studies. Section 5 concludes.

2. Methods

2.1. Mean Square Slope Definition

An estimate of the wave mean square slope can be computed from a frequency spectrum as (e.g., Ticona Rollano et al., 2019),

$$\text{mss} = \int_{f_{\min}}^{f_{\max}} \frac{(2\pi f)^4 E(f)}{g^2} df \tag{1}$$

Here f represents the wave frequency, $E(f)$ is the energy density, and g is the acceleration of gravity. This expression is directly proportional to slope squared $(ak)^2$ using the linear dispersion relationship in the deep water limit, $(2\pi f)^2 = gk$, and with $E(f) \propto a^2$. The definite integral represents an estimate of the mean square slope over a frequency extent defined by its minimum and maximum frequencies, $f_{\min}$ and $f_{\max}$. Here, the limits are taken as the lowest and highest reported frequencies of the spectrum resolvable by the finite-sized wave buoy, $f_{\min} = 0.0293$ Hz to $f_{\max} = 0.5$ Hz in $n = 38$ discrete bands, where the upper limit is set by the hydrodynamic response of the hull. We emphasize that this mean square slope metric characterizes the shape and slope contributions of the

energetic scales of the spectrum, but cannot account for waves shorter than approximately 6.3 m in wavelength (see Section 4.1).

2.2. Spotter Wave Buoy

Wave measurements were collected by free-drifting Spotter buoys (Sofar Ocean) which use GPS-derived motions to report hourly records of surface wave statistics in the form of scalar energy spectra and directional moments (Raghukumar et al., 2019). Raw data are collected at a 2.5 Hz sampling rate and processed into 256-sample FFTs to produce spectral estimates spanning 0.0293–0.5 Hz in 38 bins. A constant frequency resolution of $df = 2.5/256$ Hz is used up to 0.33 Hz, beyond which the resolution is coarsened to 3 df to reduce the size of the processed data which are transmitted hourly over the Iridium network. The sphere-like hull is 42 cm in diameter with a mass of 7.5 kg including ballast.

Spotter data is collected through a combination of targeted deployments and opportunistic measurements from Sofar's spotter network—a large, persistent-array of free-drifting Spotter buoys (Houghton et al., 2021). The density of the deployed arrays and Sofar's network help to overcome the sparsity of moored buoy arrays when targeting hurricanes. The smaller hull size also has a good response to shorter waves, which can be underestimated by some larger buoys in the National Data Buoy Center network (Jensen et al., 2021).

2.3. COAMPS-TC Model

Surface wind field estimates are derived from real-time operational forecasts made by the U.S. Naval Research Laboratory's (NRL) Coupled Ocean-Atmosphere Mesoscale Prediction System for Tropical Cyclones (COAMPS-TC) (Doyle et al., 2012, 2014). COAMPS-TC is a regional model which uses an outer fixed grid mesh (36-km horizontal resolution) and two nested storm-following grid meshes (12- and 4-km resolution) with 40 vertical levels ranging in altitude from 10 m above the surface to approximately 30 km. When producing real-time operational forecasts, the version of COAMPS-TC used in this study utilizes the NOAA Global Forecast System (GFS) analysis and forecasts for the initial and boundary conditions. For storms that have intensities greater or equal to 55 knots (28.3 m s^{-1}), the horizontal wind structure at the initial time of the model is generated from a modified Rankine wind vortex model combined with both physical and synthetic observations ingested from the National Hurricane Center. For time periods when the storm intensity is less than 55 knots at the initialization time, the initial TC vortex is downscaled from the NOAA GFS analysis.

Hourly 10-m winds from the inner-most 4-km grid are derived by aggregating successive forecasts leaving out the first 4 hr of each forecast to minimize the effect of model state adjustments that occur early in each forecast. The 10-m winds are instantaneous values (representative of a 1–10 min average) and gustiness is not resolved. Wind output is interpolated onto Spotter wave observations to produce wind-wave datasets in Hurricanes Fiona and Ian (2022).

2.4. Targeted Deployment Measurements in Hurricane Ian (2022)

Hurricane Ian was a Category 4 hurricane that caused widespread damage to both Cuba and the Southeastern United States during late September 2022. Ahead of Ian's first U.S. landfall on the Southwest coast of Florida, the continental shelf was seeded with an array of drifting buoys in a targeted deployment by an NP-3C aircraft (Figure 1) operated by Naval squadron VXS-1. Observations from six Spotter buoys in the array are co-located with wind fields from COAMPS-TC to create a data set of 432 hourly wave measurements and modeled wind speeds from 27 to 30 September 2022. Wave observations span 2–11.8 m significant wave height and 5–13 s peak period, and mostly lie between the 30 and 100 m depth contours, approximately 90–275 km offshore (see Figure S3 in Supporting Information S1). The maximum COAMPS-TC wind speed at the time and location of a Spotter observation is 52.5 m s^{-1} (117 mph).

2.5. Sofar Spotter Network Measurements in Hurricane Fiona (2022)

Hurricane Fiona was a destructive hurricane that formed in mid-September 2022 and made landfall in Puerto Rico and the Dominican Republic before traveling Northward across the Atlantic, peaking in intensity as a Category 4, then striking Eastern Canada as an extratropical cyclone. Fiona's track through the open Atlantic intersected

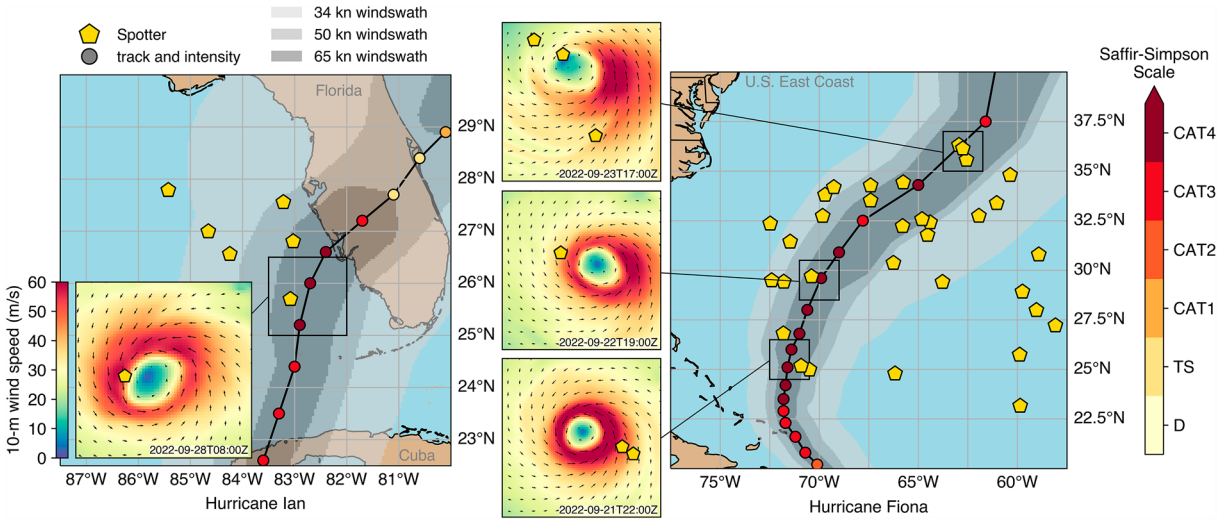

Figure 1. Buoy locations and storm track for (left) Hurricane Ian and (right) Hurricane Fiona. Storm tracks are colored by intensity, as categorized by the Saffir-Simpson scale, and the surrounding wind swaths are shaded by wind speed threshold. The insets highlight several buoy-storm interactions using 10-m wind speeds from COAMPS-TC.

with several buoys in Sofar's Spotter network. The 2772 hourly observations from 33 Spotters (Figure 1) contain measurements up to 17.5 m significant wave height and 20.5 s peak period, with a maximum interpolated model wind speed of 54.4 m s^{-1} (122 mph).

3. Results

3.1. Mean Square Slope Versus Wind Speed

At low-to-moderate wind speeds (<15 m s^{-1}), observed mean square slopes have a linear dependence on 10-m surface-level wind speed (Figure 2). This result is qualitatively consistent with the measurements of Cox and Munk (1954) at wind speeds of 2–14 m s^{-1}.

At higher wind speeds (>15 m s^{-1}), the increases in observed mss are much smaller. This trend persists through the extent of available buoy data, up to the maximum wind speed of 54.4 m s^{-1} (122 mph) as modeled by

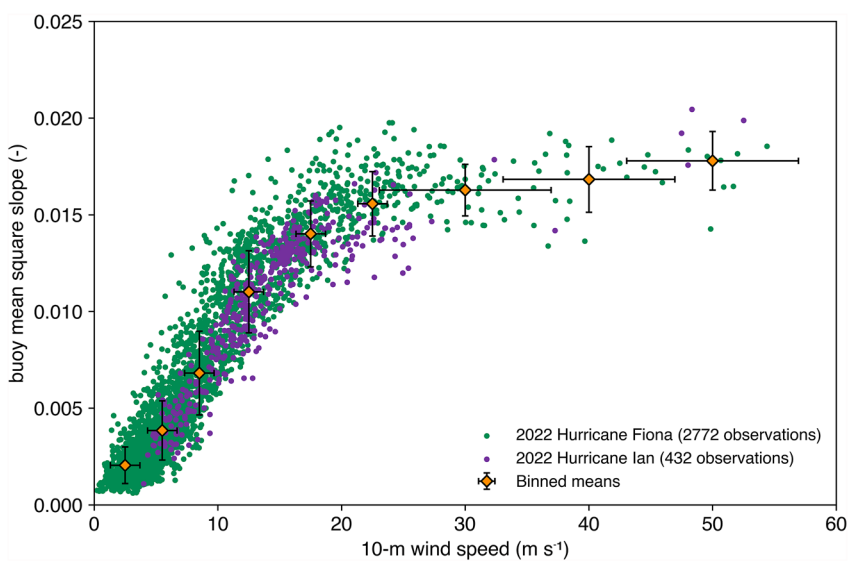

Figure 2. Spotter mean square slope from wave measurements in Hurricanes Ian and Fiona as a function of COAMPS-TC 10-m wind speed. Bin centers represent the mean and standard deviation of mean square slope in each bin.

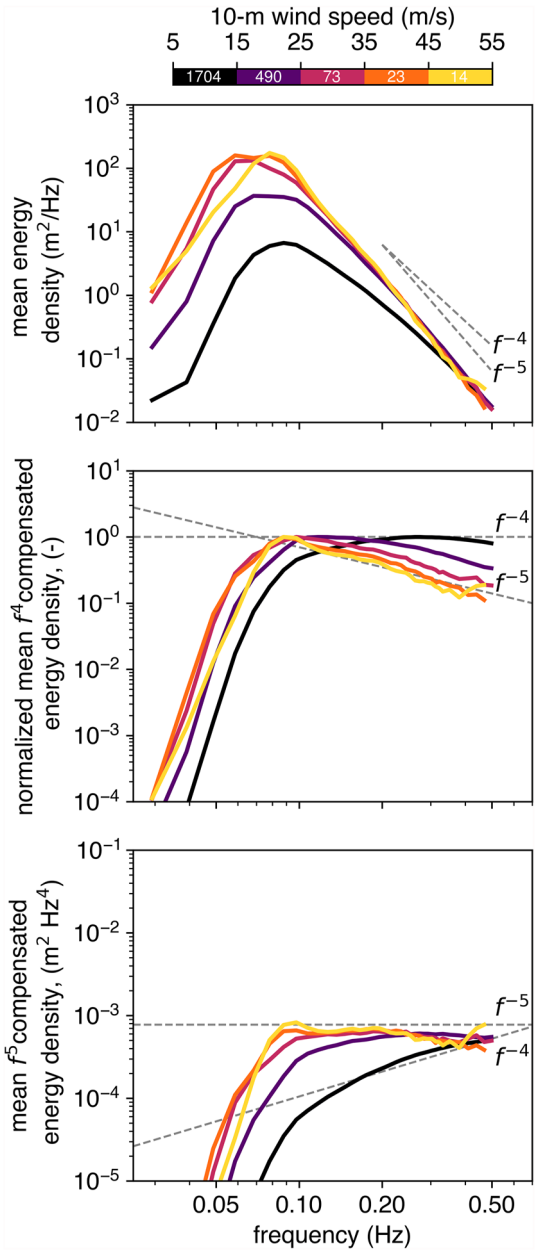

Figure 3. Upper panel: mean energy density in 10 m s^{-1} bins. Bin counts (1-hr spectra) are labeled inside of the color bar. Middle panel: the mean energy spectra compensated by f^4 (as $energy \cdot f^4$) and normalized by their respective maximum value. In such a scaling, f^{-4} trends collapse to a constant line (as indicated by the correspondingly labeled dashed line). Lower panel: mean energy spectra compensated by f^5.

COAMPS-TC. Bin centers represent the mean and standard deviation of mss in each bin. Lateral uncertainty in the wind speed is estimated using COAMPS-TC 6-hr forecast error relative to the National Hurricane Center best track re-analysis. A 7 m s^{-1} error is placed on high wind speeds, near the radius of maximum winds, which derives from the standard deviation of the distribution of COAMPS-TC 6-hr intensity errors evaluated for hundreds of major hurricane forecasts. A 1.2 m s^{-1} error is used at lower wind speeds, located in the outer part of the storm, and is estimated from an error distribution created by shifting the COAMPS-TC forecast on top of the best track position and comparing the updated wind speed at the buoy's position to the originally-forecasted wind speed.

Ticona Rollano et al. (2019) observed wave slope saturation with wind speed starting at 11 m s^{-1} and noted the behavior to be qualitatively similar to the saturation of measured turbulent dissipation in the ocean surface layer. In wind-wave flume experiments, Troitskaya et al. (2012) found wave slope to have a tendency toward saturation which was coincident with saturation of the laboratory air-sea drag coefficient above wind speeds of 25 m s^{-1}. The authors attribute the decrease in slope to the "tearing of the wave crests at severe wind conditions." In the University of Miami Wave Model, there is a similar transition in mean square slopes at high winds, though the values do not fully saturate (Donelan, 2018). A more complete comparison with other mss results from the literature is given in the discussion (Section 4.1).

3.2. Spectral Shape Change With Wind Speed

Mean square slope is a measure of both the physical wave slope (a^2k^2) as well the wave spectral shape (i.e., as the fourth moment of the spectrum). The evolution of the observed wave spectra with wind speed is shown in Figure 3 as the mean energy density in 10 m s^{-1} bins. At low-to-moderate wind speeds (<15 m s^{-1}), the spectral tail above 0.10 Hz follows the canonical f^{-4} slope expected of the equilibrium range (wind input, dissipation from breaking, and nonlinear energy fluxes in balance).

From 15 to 25 m s^{-1}, the frequency extent of the equilibrium range is shorter and the tail of the spectrum, from 0.2 Hz onward, transitions to the f^{-5} slope characteristic of the dissipation range (wind input balanced solely by dissipation). This change is coincident with the weakening of the wind speed dependence of mss in Figure 2. The equilibrium range (f^{-4}) continues to narrow with increasing wind speed, until the spectral tail is almost entirely dominated by the dissipation range (f^{-5}) at the most extreme winds (45–55 m s^{-1}). For any given total wave energy (or significant wave height), the change in spectra shape to f^{-5} results in a reduction in mss, relative to an f^{-4} shape with the same total energy. Though much of this energy is contained in lower frequencies of the spectrum, changes in the high frequency tail have the highest influence on the mss integral due to the f^4 dependence of Equation 1. Thus, wave heights can continue to increase with increasing wind speed, while mss saturates. The growth of the peak wavelength as a function of wind speed is specific to the evolution of a storm, but approaches 200–300 m near 40 m s^{-1} for both hurricanes (Figure S14 in Supporting Information S1).

The spectral slopes are in general agreement with the large number of hurricane wave observations collected by Tamizi and Young (2020) which vary from f^{-4} to f^{-5}. Observations of the transition in spectral tail slope from f^{-4} to f^{-5} by Vincent et al. (2019) and Lenain and Melville (2017) demonstrate the transition frequency (and wavenumber) decreases with increasing wind speed (in wind speeds up to 20 m s^{-1}). While neither result extends to the extreme, 55 m s^{-1} wind speeds observed here, the transition frequency appears to decay exponentially with an apparent asymptote at 0.30 Hz in the Vincent et al. (2019) data (max winds 20 m s^{-1}).

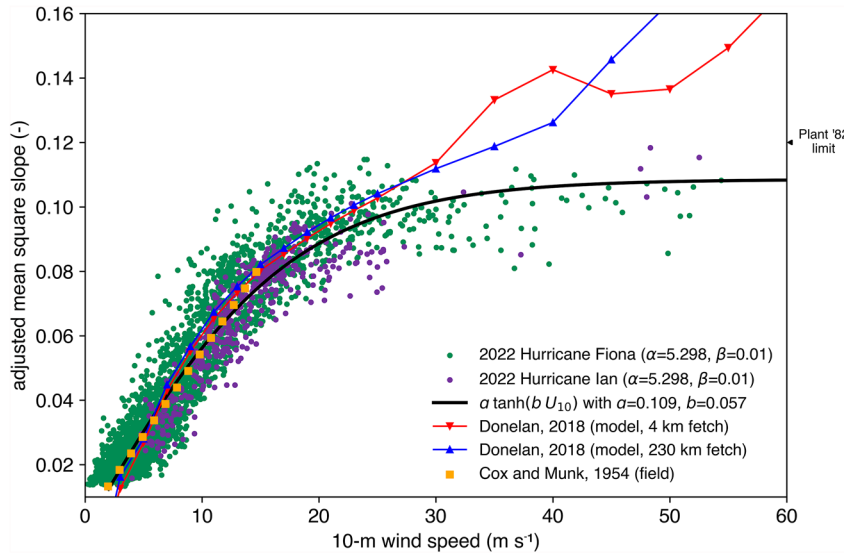

Figure 4. Adjusted mean square slope, calculated from Equation 2 with $\alpha = 5.3$ and $\beta = 0.01$ using wave measurements in Hurricanes Ian and Fiona, as a function of model 10-m wind speed. An $a\tanh(bU_{10})$ fit is shown with $a = 0.109$ and $b = 0.057$. The classic field measurements of Cox and Munk (1954) are superimposed along with the University of Miami Wave Model slope estimates at fetches of 4 and 230 km from Donelan (2018).

Spectra with a narrow f^{-4} range and dominant f^{-5} tail are present in the SWIFT buoy observations of Schwendeman et al. (2014). The authors note the SWIFT spectra derive from young, highly forced waves (which is the case here) as defined by the wave age, or the ratio of wave phase speed to the 10-m wind speed. This trend is in agreement with the results of Romero and Melville (2010) that demonstrate a narrowing of the equilibrium range with decreasing wave age. Spotter spectra, binned by wave age, are shown in the supplement (Figure S1 in Supporting Information S1) and are consistent with this wave age dependence.

4. Discussion

4.1. Limitations of Wave Scales Observed by Buoys

It is well known that buoys cannot measure waves shorter than a few meters because the hydrodynamic response of their hull is limited to frequencies higher than the natural frequency (typically 0.5–1.0 Hz, see Thomson et al. (2015) for details). At low-to-moderate wind speeds and wave conditions, a substantial portion of the total mean square slope is supported by shorter waves only measurable by methods such as lidar (Lenain et al., 2019; Lenain & Melville, 2017) and polarimetry (Zappa et al., 2008). The buoy mss can be partially corrected by incorporating empirical parameters into Equation 1 which effectively extrapolate the spectra to higher frequencies,

$$\text{adjusted mss} = \alpha \int_{f_{\min}}^{f_{\max}} \frac{(2\pi f)^4 E(f)}{g^2} df + \beta. \quad (2)$$

The empirical factors α and β are introduced to account for the mean square slope contributions of the higher frequency waves not resolvable by the Spotter buoy (i.e., waves shorter than $f_{\max} = 0.5$ Hz or 6.3 m in wavelength). Fitting α in Equation 2 to Cox and Munk (1954) over the linear regime of Figure 4 (from 2 to 15 m s^{-1}) yields $\alpha = 5.3$ with an offset of $\beta = 0.01$.

In Figure 4, adjusted mss (with $\alpha = 5.3$ and $\beta = 0.01$) is compared to the data of Cox and Munk as well as the slopes modeled by Donelan (2018) using the University of Miami Wave Model. The Miami wave model includes the full spectrum of gravity, capillary-gravity and capillary waves in prescribing mss. In this same figure, a tanh function is fit to the data with coefficients $a = 0.109 \pm 0.0009$ and $b = 0.057 \pm 0.0007$ s m^{-1} and a root mean square error of 0.0086. In all datasets, the transition to a regime with weaker mss dependence on wind speed is observed near 15 m s^{-1}, corresponding to an approximate slope of 0.08 or $\tan(16\,\text{deg})^2$ as identified by Cox and Munk (1954). The adjusted mss and Donelan results are in good agreement up to a wind speed of 30 m s^{-1}.

Beyond that, the Donelan model results exceed the Hurricane Ian and Fiona observations by 15%–30%. At high winds (>30 m s^{-1}), the model exhibits a sensitivity to fetch (which is beyond the scope of the present study). Interestingly, the adjusted buoy mss in Figure 4 appear capped by the upper limit on omnidirectional mean square slope proposed by Plant (1982), $mss_{max} = 0.08 \pm 0.04$, or using the upper value, $mss_{max} = 0.12$. The limit is proposed based on requirement that the flux of momentum from wind to waves should not exceed the wind stress for wave growth proportional to $(u^*/c)^2$ (ratio of friction velocity to wave phase speed, squared), and is employed by Elfouhaily et al. (1997) to vet several candidates for parametric spectra.

While useful for a rough comparison of buoy mss to slopes calculated over larger frequency extents, there remains large uncertainty in the use of α and β to correct buoy mss to total mss. The coefficient α is biased when the transition from the equilibrium range to the dissipation range (Figure 3) is well within the frequencies resolvable by the buoy, which occurs around wind speeds of 15–20 m s^{-1}, since the contribution to mss of a saturated portion of the spectrum is less significant than that of an equilibrium portion of the spectrum (or similarly higher-sloped portion). An alternative approach is to extend the observed f^{-5} tail, however this would not capture the evolution of the wave spectrum in the gravity-capillary range (wavelengths less than 1 m down to several millimeters) which changes shape with increasing wind speed (Laxague et al., 2018; Zappa et al., 2008). A parametric tail, for example, Elfouhaily et al. (1997), could be imposed, but many parameterizations are developed on wind speeds not exceeding 20 m s^{-1}.

In future work, the NOAA Wide Swath Radar Altimeter (WSRA) and Stepped Frequency Microwave Radiometer (SFMR) instruments are good candidates for producing relevant datasets of hurricane winds and waves (Klotz & Uhlhorn, 2014; Walsh et al., 2021). The WSRA measures wave topography (which can be used to compute mss) and SFMR provides a measure of surface wind speed. Both fly concurrently aboard the NOAA WP-3D aircraft during Hurricane Hunter missions.

4.2. Considerations for Free-Drifting Platforms

A free-drifting, buoy-based observation of wave steepness fundamentally relies on time series and thus frequency analysis. Doppler shift of the observed wave spectrum can occur when a measurement platform propels in or against waves (Collins et al., 2017) or when waves pass through gradients in surface currents (Iyer et al., 2022). At high wind speeds, it is unlikely that such waves can exist without the presence of a surface currents. The Spotter buoys make observations in a predominantly wave-following, intrinsic reference frame. A Doppler correction would be necessary to compare these results with a measurement from a fixed reference frame. Future studies should focus on a direct measurement of slope using other technologies.

4.3. Implications for Surface Drag Coefficient

The air-sea drag coefficient, which governs the rate of momentum transfer between the air and ocean surface, depends on the surface roughness length under neutral stability (Charnock, 1955). Using a groundbreaking set of GPS sonde tropical cyclone field measurements, Powell et al. (2003) observed a saturation and eventual reduction in both roughness length and drag coefficient at extreme wind speeds. More recent studies have verified this result and added functional dependencies (e.g., Holthuijsen et al., 2012). The subsequent adoption of a reduced drag coefficient in models has been essential to improving tropical cyclone intensity forecasts (e.g., C. Davis et al., 2008). The evolution of mean square slope presented here is qualitatively similar, increasing steadily through moderate winds before leveling-off at higher wind speeds. Taylor and Yelland (2001) demonstrated the ability of a roughness length scaling based on bulk wave slope (H_s/L_p, or the ratio of significant wave height to peak wavelength) to predict observed roughness across a wide range of datasets, including the open ocean. This bulk steepness is closely related to mss and shares a tendency to saturate at high wind speeds in our data, as shown in Figure S12 of Supporting Information S1. Takagaki et al. (2012) report a similar H/L roughness dependence in the lab. The roughness length dependence wave slope, combined with the saturation of slopes at high wind speeds observed here, might thus contribute to the reduction of the drag coefficient at hurricane force wind speeds.

The observed progression of spectral shape can be directly linked to sea-state dependent drag. Plant (1982) hypothesized a wave growth function proportional to $(u^*/c)^2$ where the friction velocity u^* is a function of the wave energy spectrum within the equilibrium range of the spectral tail (Phillips, 1985). Here, the f^{-4} equilibrium range narrows rapidly for winds exceeding 25 m s^{-1} and is replaced by the f^{-5} dissipative range, leading to

enhanced wave breaking. In addition to limiting wave steepness, intense wave breaking promotes the generation of spray, which becomes increasingly present within a multi-phase surface foam layer and is hypothesized to modulate the drag coefficient for winds above 30 m s^{-1} (Holthuijsen et al., 2012; Hwang, 2018; Troitskaya et al., 2016, 2019, and others). Recently, Lan et al. (2022) achieved notable tropical cyclone model skill improvement through the use of a roughness parameterization that depends both on sea state and foam, employing the Taylor and Yelland (2001) slope scaling at low wave ages (<15.2) and the Drennan et al. (2003) wave age scaling at higher wave ages.

Though a mean square slope integrated to frequencies beyond the buoy observations might be necessary for a direct relation to the skin friction component of the drag coefficient, the slope of the waves measured by buoys remains important to the understanding of form drag and pressure work (Donelan, 2018; Kudryavtsev & Makin, 2007, and others). The buoy measurements, though lacking the very highest frequency waves, include the vast majority of the total energy in the wave spectrum. More practically, the buoy measurements are the wave information most readily available for real-time assimilation into coupled forecast models.

4.4. Secondary Dependencies of mss at High Winds

Although this set of buoy data has been sufficient to determine a parametric relation between mss and wind speed, it has not been sufficient to determine secondary dependencies. Building on ideas from the literature, we have tested the residual scatter from a tanh fit of the data in Figure 2 for dependence on storm quadrant (position relative to the center and heading of the storm), wind-wave alignment, wave age, and storm speed. While none of these tests show a statistically significant result, there are some possible signals. When viewing the time series of each individual buoy rather than the aggregated data, the mss values are higher for a given wind speed when the winds and waves are well-aligned. The alignment dependence would be consistent with formulations for wind-wave growth that utilize the wind stress vector and the wave celerity vector (Gemmrich et al., 1994). Porchetta et al. (2019) found alignment can improve the parameterization of roughness length, observing an increase in roughness with large misalignment, though the authors report it has almost no effect in young waves. Depth also plays a role in the transformation of waves in shallow water, however spectrograms of relative depth indicate that the frequencies of interest to mss, 0.10 Hz and above, remain above the deep water limit (Figure S3 in Supporting Information S1). Dependency on storm quadrant may be obscured by COAMPS-TC track position errors, though the standard deviation of 6-hr track errors (based on hundred of major hurricane forecasts) is 21 km, likely not large enough to place a buoy at the edge of the eyewall on the other side of the eye. Time series figures are included in the Supporting Information S1.

5. Conclusions

Ocean surface wave buoy measurements within two hurricanes show a consistent regime change in the relation of wave slopes to wind speeds. Up to moderate wind speeds (<15 m s^{-1}), wave slopes increase linearly with wind speed, as has been documented in the literature. At higher wind speeds, wave slopes appear to reach an upper limit, with no further increase beyond 30 m s^{-1} winds. The upper limit is similar to a heuristic value of 0.12 proposed by Plant (1982). This mss limit is directly related to the emergence of an f^{-5} dissipation (saturation) range as the dominant shape of the scalar wave energy spectra under high wind speeds. The wave slope changes are likely related to changes in the surface drag coefficient, for which a more comprehensive data set is needed to evaluate. A larger data set of wave observations in more hurricanes will be valuable for considering secondary effects, such as dependencies on storm quadrant, wind-wave alignment, the interaction between swell and wind-sea, and storm speed.

Data Availability Statement

The wind and wave data used in this work are publicly available at Dryad via https://doi.org/10.5061/dryad.g4f4qrfvb (J. R. Davis et al., 2023). The storm track and speed data used to test secondary dependencies were sourced from IBTrACS (Knapp et al., 2010, 2018). Shapefiles of the storm track and wind swaths used in the maps are from the National Hurricane Center GIS Archive available at https://www.nhc.noaa.gov/gis/.

Acknowledgments
This work was funded by the U.S. National Ocean Partnership Program (NOPP) as part of the NOPP Coastal Hurricane Impacts project (ONR Grant N00014-21-1-2194). Co-authors Doyle, Komaromi, and Moskaitis gratefully acknowledge support from Office of Naval Research grant Program Element 0601153N. Computational resources for the COAMPS-TC forecasts were provided by the Navy Department of Defense Supercomputing Resource Center in Stennis, Mississippi. Air-support was provided by the Navy VXS-1 Scientific Deployment Squadron via the Naval Research Laboratory. The Spotter global network data was provided by Sofar Ocean. This material is based upon work supported by the National Science Foundation Graduate Research Fellowship Program under Grant DGE-2140004. Any opinions, findings, and conclusions or recommendations expressed in this material are those of the author(s) and do not necessarily reflect the views of the National Science Foundation.

References

Banner, M. L. (1990). Equilibrium spectra of wind waves. *Journal of Physical Oceanography*, *20*(7), 966–984. https://doi.org/10.1175/1520-0485(1990)020<0966:esoww>2.0.co;2

Bréon, F. M., & Henriot, N. (2006). Spaceborne observations of ocean glint reflectance and modeling of wave slope distributions. *Journal of Geophysical Research*, *111*(C6), C06005. https://doi.org/10.1029/2005JC003343

Bruciaferri, D., Tonani, M., Lewis, H. W., Siddorn, J. R., Saulter, A., Castillo, J. M., et al. (2021). The impact of ocean-wave coupling on the upper ocean circulation during storm events. *Journal of Geophysical Research: Oceans*, *126*(6), e2021JC017343. https://doi.org/10.1029/2021JC017343

Charnock, H. (1955). Wind stress on a water surface. *Quarterly Journal of the Royal Meteorological Society*, *81*(350), 639–640. https://doi.org/10.1002/qj.49708135027

Cline, I. M. (1920). Relation of changes in storm tides on the coast of the Gulf of Mexico to the center and movement of hurricanes. *Monthly Weather Review*, *48*(3), 127–146. https://doi.org/10.1175/1520-0493(1920)48<127:rocist>2.0.co;2

Collins, C. O., Blomquist, B., Persson, O., Lund, B., Rogers, W. E., Thomson, J., et al. (2017). Doppler correction of wave frequency spectra measured by underway vessels. *Journal of Atmospheric and Oceanic Technology*, *34*(2), 429–436. https://doi.org/10.1175/JTECH-D-16-0138.1

Collins, C. O., Potter, H., Lund, B., Tamura, H., & Graber, H. C. (2018). Directional wave spectra observed during intense tropical cyclones. *Journal of Geophysical Research: Oceans*, *123*(2), 773–793. https://doi.org/10.1002/2017JC012943

Cox, C., & Munk, W. (1954). Measurement of the roughness of the sea surface from photographs of the Sun's glitter. *Journal of the Optical Society of America*, *44*(11), 838. https://doi.org/10.1364/JOSA.44.000838

Davis, C., Wang, W., Chen, S. S., Chen, Y., Corbosiero, K., DeMaria, M., et al. (2008). Prediction of landfalling hurricanes with the advanced hurricane WRF model. *Monthly Weather Review*, *136*(6), 1990–2005. https://doi.org/10.1175/2007MWR2085.1

Davis, J. R., Thomson, J., Houghton, I., Doyle, J. D., Komaromi, W., Moskaitis, J., et al. (2023). Data to accompany the article "saturation of ocean surface wave slopes observed during hurricanes" [Dataset]. Dryad. https://doi.org/10.5061/dryad.g4f4qrfvb

Donelan, M. A. (2018). On the decrease of the oceanic drag coefficient in high winds. *Journal of Geophysical Research: Oceans*, *123*(2), 1485–1501. https://doi.org/10.1002/2017JC013394

Doyle, J., Hodur, R., Chen, S., Jin, Y., Msokaitis, J., Wang, S., et al. (2014). Tropical cyclone prediction using COAMPS-TC. *Oceanography*, *27*(3), 104–115. https://doi.org/10.5670/oceanog.2014.72

Doyle, J., Jin, Y., Hodur, R. M., Chen, S., Jin, H., Moskaitis, J., et al. (2012). In *Real-time tropical cyclone prediction using COAMPS-TC* (pp. 15–28). https://doi.org/10.1142/9789814405683_0002

Drazen, D. A., Melville, W. K., & Lenain, L. (2008). Inertial scaling of dissipation in unsteady breaking waves. *Journal of Fluid Mechanics*, *611*, 307–332. https://doi.org/10.1017/S0022112008002826

Drennan, W. M., Graber, H. C., Hauser, D., & Quentin, C. (2003). On the wave age dependence of wind stress over pure wind seas. *Journal of Geophysical Research*, *108*(C3), 8062. https://doi.org/10.1029/2000JC000715

Duncan, J. H. (1981). An experimental investigation of breaking waves produced by a towed hydrofoil. *Proceedings of the Royal Society of London. A. Mathematical and Physical Sciences*, *377*(1770), 331–348. https://doi.org/10.1098/rspa.1981.0127

Elfouhaily, T., Chapron, B., Katsaros, K., & Vandemark, D. (1997). A unified directional spectrum for long and short wind-driven waves. *Journal of Geophysical Research*, *102*(C7), 15781–15796. https://doi.org/10.1029/97JC00467

Forristall, G. Z. (1981). Measurements of a saturated range in ocean wave spectra. *Journal of Geophysical Research*, *86*(C9), 8075. https://doi.org/10.1029/JC086iC09p08075

Gemmrich, J., Mudge, T., & Polonichko, V. (1994). On the energy input from wind to surface waves. *Journal of Physical Oceanography*, *24*(11), 2413–2417. https://doi.org/10.1175/1520-0485(1994)024<2413:oteifw>2.0.co;2

Guérin, C.-A., Capelle, V., & Hartmann, J.-M. (2022). Revisiting the Cox and Munk wave-slope statistics using IASI observations of the sea surface. *Remote Sensing of Environment*, *288*, 113508.

Hegermiller, C. A., Warner, J. C., Olabarrieta, M., & Sherwood, C. R. (2019). Wave–current interaction between Hurricane Matthew wave fields and the Gulf Stream. *Journal of Physical Oceanography*, *49*(11), 2883–2900. https://doi.org/10.1175/JPO-D-19-0124.1

Hell, M. C., Ayet, A., & Chapron, B. (2021). Swell generation under extra-tropical storms. *Journal of Geophysical Research: Oceans*, *126*(9), e2021JC017637. https://doi.org/10.1029/2021JC017637

Holthuijsen, L. H., Powell, M. D., & Pietrzak, J. D. (2012). Wind and waves in extreme hurricanes. *Journal of Geophysical Research*, *117*(C9), C09003. https://doi.org/10.1029/2012JC007983

Houghton, I., Smit, P., Clark, D., Dunning, C., Fisher, A., Nidzieko, N., et al. (2021). Performance statistics of a real-time Pacific Ocean weather sensor network. *Journal of Atmospheric and Oceanic Technology*, *38*(5), 1047–1058. https://doi.org/10.1175/JTECH-D-20-0187.1

Hsu, J.-Y. (2021). Observing surface wave directional spectra under Typhoon Megi (2010) using subsurface EM-APEX floats. *Journal of Atmospheric and Oceanic Technology*, *38*(11), 1949–1966. https://doi.org/10.1175/JTECH-D-20-0210.1

Hsu, J.-Y., Lien, R.-C., D'Asaro, E. A., & Sanford, T. B. (2019). Scaling of drag coefficients under five tropical cyclones. *Geophysical Research Letters*, *46*(6), 3349–3358. https://doi.org/10.1029/2018GL081574

Hsu, S. A., Yijun, H., & Shen, H. (2017). Buoy measurements of wind–wave relations during Hurricane Matthew in 2016. *Journal of Physical Oceanography*, *47*(10), 2603–2609. https://doi.org/10.1175/JPO-D-16-0280.1

Hwang, P. A. (2016). Fetch- and duration-limited nature of surface wave growth inside tropical cyclones: With applications to air–sea exchange and remote sensing. *Journal of Physical Oceanography*, *46*(1), 41–56. https://doi.org/10.1175/JPO-D-15-0173.1

Hwang, P. A. (2018). High-wind drag coefficient and whitecap coverage derived from microwave radiometer observations in tropical cyclones. *Journal of Physical Oceanography*, *48*(10), 2221–2232. https://doi.org/10.1175/JPO-D-18-0107.1

Hwang, P. A., & Fan, Y. (2017). Effective fetch and duration of tropical cyclone wind fields estimated from simultaneous wind and wave measurements: Surface wave and air–sea exchange computation. *Journal of Physical Oceanography*, *47*(2), 447–470. https://doi.org/10.1175/JPO-D-16-0180.1

Hwang, P. A., & Walsh, E. J. (2018). Propagation directions of ocean surface waves inside tropical cyclones. *Journal of Physical Oceanography*, *48*(7), 1495–1511. https://doi.org/10.1175/JPO-D-18-0015.1

Iyer, S., Thomson, J., Thompson, E., & Drushka, K. (2022). Variations in wave slope and momentum flux from wave-current interactions in the tropical trade winds. *Journal of Geophysical Research: Oceans*, *127*(3), e2021JC018003. https://doi.org/10.1029/2021JC018003

Janssen, P. A. E. M., & Bidlot, J.-R. (2023). Wind–wave interaction for strong winds. *Journal of Physical Oceanography*, *53*(3), 779–804. https://doi.org/10.1175/JPO-D-21-0293.1

Jensen, R. E., Swail, V., & Bouchard, R. H. (2021). Quantifying wave measurement differences in historical and present wave buoy systems. *Ocean Dynamics*, *71*(6–7), 731–755. https://doi.org/10.1007/s10236-021-01461-0

King, D. B., & Shemdin, O. H. (1978). Radar observation of hurricane wave directions. In *Coastal Engineering 1978* (pp. 209–226). American Society of Civil Engineers. https://doi.org/10.1061/9780872621909.012

Kita, Y., & Waseda, T. (2022). Ocean surface wave effects on development of explosive cyclone. *Earth and Space Science Open Archive*, *35*. https://doi.org/10.1002/essoar.10510382.1

Klotz, B. W., & Uhlhorn, E. W. (2014). Improved stepped frequency microwave radiometer tropical cyclone surface winds in heavy precipitation. *Journal of Atmospheric and Oceanic Technology*, *31*(11), 2392–2408. https://doi.org/10.1175/JTECH-D-14-00028.1

Knapp, K. R., Diamond, H. J., Kossin, J. P., Kruk, M. C., & Schreck, C. J. (2018). International Best Track Archive for Climate Stewardship (IBTrACS) Project, version 04r00 [Dataset]. National Centers for Environmental Information. https://doi.org/10.25921/82ty-9e16

Knapp, K. R., Kruk, M. C., Levinson, D. H., Diamond, H. J., & Neumann, C. J. (2010). The International Best Track Archive for Climate Stewardship, (IBTrACS): Unifying tropical cyclone best track data. *Bulletin of the American Meteorological Society*, *91*(3), 363–376. https://doi.org/10.1175/2009BAMS2755.1

Kudryavtsev, V., Golubkin, P., & Chapron, B. (2015). A simplified wave enhancement criterion for moving extreme events. *Journal of Geophysical Research: Oceans*, *120*(11), 7538–7558. https://doi.org/10.1002/2015JC011284

Kudryavtsev, V., & Makin, V. (2007). Aerodynamic roughness of the sea surface at high winds. *Boundary-Layer Meteorology*, *125*(2), 289–303. https://doi.org/10.1007/s10546-007-9184-7

Lan, Y., Sun, D., Leng, H., Song, J., Cao, X., & Dong, R. (2022). A new sea surface roughness parameterization and its application in tropical cyclone modeling. *Journal of Geophysical Research: Atmospheres*, *127*(24), e2022JD037159. https://doi.org/10.1029/2022JD037159

Laxague, N. J. M., Zappa, C. J., LeBel, D. A., & Banner, M. L. (2018). Spectral characteristics of gravity-capillary waves, with connections to wave growth and microbreaking. *Journal of Geophysical Research: Oceans*, *123*(7), 4576–4592. https://doi.org/10.1029/2018JC013859

Lenain, L., & Melville, W. K. (2017). Measurements of the directional spectrum across the equilibrium saturation ranges of wind-generated surface waves. *Journal of Physical Oceanography*, *47*(8), 2123–2138. https://doi.org/10.1175/JPO-D-17-0017.1

Lenain, L., Statom, N. M., & Melville, W. K. (2019). Airborne measurements of surface wind and slope statistics over the ocean. *Journal of Physical Oceanography*, *49*(11), 2799–2814. https://doi.org/10.1175/JPO-D-19-0098.1

Li, X., Karaev, V., Panfilova, M., Liu, B., Wang, Z., Xu, Y., et al. (2022). Measurements of total sea surface mean square slope field based on SWIM data. *IEEE Transactions on Geoscience and Remote Sensing*, *60*, 1–9. https://doi.org/10.1109/TGRS.2022.3174392

Melville, W. K. (1994). Energy dissipation by breaking waves. *Journal of Physical Oceanography*, *24*(10), 2041–2049. https://doi.org/10.1175/1520-0485(1994)024<2041:edbbw>2.0.co;2

Patterson, M. M. (1974). Oceanographic data from Hurricane Camille. In *Offshore Technology Conference. Houston, Texas*. https://doi.org/10.4043/2109-MS

Phillips, O. M. (1985). Spectral and statistical properties of the equilibrium range in wind-generated gravity waves. *Journal of Fluid Mechanics*, *156*, 505–531. https://doi.org/10.1017/S0022112085002221

Plant, W. J. (1982). A relationship between wind stress and wave slope. *Journal of Geophysical Research*, *87*(C3), 1961. https://doi.org/10.1029/JC087iC03p01961

Porchetta, S., Temel, O., Muñoz-Esparza, D., Reuder, J., Monbaliu, J., Van Beeck, J., & Van Lipzig, N. (2019). A new roughness length parameterization accounting for wind–wave (mis)alignment. *Atmospheric Chemistry and Physics*, *19*(10), 6681–6700. https://doi.org/10.5194/acp-19-6681-2019

Powell, M. D., Vickery, P. J., & Reinhold, T. A. (2003). Reduced drag coefficient for high wind speeds in tropical cyclones. *Nature*, *422*(6929), 279–283. https://doi.org/10.1038/nature01481

Raghukumar, K., Chang, G., Spada, F., Jones, C., Janssen, T., & Gans, A. (2019). Performance characteristics of "Spotter," a newly developed real-time wave measurement buoy. *Journal of Atmospheric and Oceanic Technology*, *36*(6), 1127–1141. https://doi.org/10.1175/JTECH-D-18-0151.1

Romero, L., Melville, W. K., & Kleiss, J. M. (2012). Spectral energy dissipation due to surface wave breaking. *Journal of Physical Oceanography*, *42*(9), 1421–1444. https://doi.org/10.1175/JPO-D-11-072.1

Romero, L., & Melville, W. K. (2010). Airborne observations of fetch-limited waves in the Gulf of Tehuantepec. *Journal of Physical Oceanography*, *40*(3), 441–465. https://doi.org/10.1175/2009JPO4127.1

Schwendeman, M., & Thomson, J. (2017). Sharp-crested breaking surface waves observed from a ship-based stereo video system. *Journal of Physical Oceanography*, *47*(4), 775–792. https://doi.org/10.1175/JPO-D-16-0187.1

Schwendeman, M., Thomson, J., & Gemmrich, J. R. (2014). Wave breaking dissipation in a young wind sea. *Journal of Physical Oceanography*, *44*(1), 104–127. https://doi.org/10.1175/JPO-D-12-0237.1

Sun, R., Villas Bôas, A. B., Subramanian, A. C., Cornuelle, B. D., Mazloff, M. R., Miller, A. J., et al. (2022). Focusing and defocusing of tropical cyclone generated waves by ocean current refraction. *Journal of Geophysical Research: Oceans*, *127*(1), e2021JC018112. https://doi.org/10.1029/2021JC018112

Takagaki, N., Komori, S., Suzuki, N., Iwano, K., Kuramoto, T., Shimada, S., et al. (2012). Strong correlation between the drag coefficient and the shape of the wind sea spectrum over a broad range of wind speeds. *Geophysical Research Letters*, *39*(23), L23604. https://doi.org/10.1029/2012GL053988

Takagaki, N., Komori, S., Suzuki, N., Iwano, K., & Kurose, R. (2016). Mechanism of drag coefficient saturation at strong wind speeds. *Geophysical Research Letters*, *43*(18), 9829–9835. https://doi.org/10.1002/2016GL070666

Tamizi, A., & Young, I. R. (2020). The spatial distribution of ocean waves in tropical cyclones. *Journal of Physical Oceanography*, *50*(8), 2123–2139. https://doi.org/10.1175/JPO-D-20-0020.1

Taylor, P. K., & Yelland, M. J. (2001). The dependence of sea surface roughness on the height and steepness of the waves. *Journal of Physical Oceanography*, *31*(2), 572–590. https://doi.org/10.1175/1520-0485(2001)031⟨0572:TDOSSR⟩2.0.CO;2

Thomson, J., D'Asaro, E. A., Cronin, M. F., Rogers, W. E., Harcourt, R. R., & Shcherbina, A. (2013). Waves and the equilibrium range at Ocean Weather Station P. *Journal of Geophysical Research: Oceans*, *118*(11), 5951–5962. https://doi.org/10.1002/2013JC008837

Thomson, J., Talbert, J., de Klerk, A., Brown, A., Schwendeman, M., Goldsmith, J., et al. (2015). Biofouling effects on the response of a wave measurement buoy in deep water. *Journal of Atmospheric and Oceanic Technology*, *32*(6), 1281–1286. https://doi.org/10.1175/JTECH-D-15-0029.1

Ticona Rollano, F., Brown, A., Ellenson, A., Özkan Haller, H. T., Thomson, J., & Haller, M. C. (2019). Breaking waves in deep water: Measurements and modeling of energy dissipation. *Ocean Dynamics*, *69*(10), 1165–1179. https://doi.org/10.1007/s10236-019-01301-2

Toba, Y. (1973). Local balance in the air-sea boundary processes. *Journal of the Oceanographical Society of Japan*, *29*(5), 209–220. https://doi.org/10.1007/bf02108528

Troitskaya, Y., Ezhova, E., Soustova, I., & Zilitinkevich, S. (2016). On the effect of sea spray on the aerodynamic surface drag under severe winds. *Ocean Dynamics*, *66*(5), 659–669. https://doi.org/10.1007/s10236-016-0948-9

Troitskaya, Y., Sergeev, D., Kandaurov, A., Vdovin, M., & Zilitinkevich, S. (2019). The effect of foam on waves and the aerodynamic roughness of the water surface at high winds. *Journal of Physical Oceanography*, *49*(4), 959–981. https://doi.org/10.1175/JPO-D-18-0168.1

Troitskaya, Y., Sergeev, D. A., Kandaurov, A. A., Baidakov, G. A., Vdovin, M. A., & Kazakov, V. I. (2012). Laboratory and theoretical modeling of air-sea momentum transfer under severe wind conditions. *Journal of Geophysical Research*, *117*(C11), C00J21. https://doi.org/10.1029/2011JC007778

Vincent, C. L., Thomson, J., Graber, H. C., & Collins, C. O. (2019). Impact of swell on the wind-sea and resulting modulation of stress. *Progress in Oceanography*, *178*, 102164. https://doi.org/10.1016/j.pocean.2019.102164

Voermans, J. J., Smit, P. B., Janssen, T. T., & Babanin, A. V. (2020). Estimating wind speed and direction using wave spectra. *Journal of Geophysical Research: Oceans*, *125*(2), e2019JC015717. https://doi.org/10.1029/2019JC015717

Walsh, E. J., Fairall, C. W., & PopStefanija, I. (2021). In the eye of the storm. *Journal of Physical Oceanography*. https://doi.org/10.1175/JPO-D-20-0219.1

Walsh, E. J., Wright, C. W., Vandemark, D., Krabill, W. B., Garcia, A. W., Houston, S. H., et al. (2002). Hurricane directional wave spectrum spatial variation at landfall. *Journal of Physical Oceanography*, *32*(6), 1667–1684. https://doi.org/10.1175/1520-0485(2002)032⟨1667:HDWSSV⟩2.0.CO;2

Whalen, J., & Ochi, M. (1978). Variability of wave spectral shapes associated with hurricanes. In *OTC Offshore Technology Conference*.

Young, I. R. (2003). A review of the sea state generated by hurricanes. *Marine Structures*, *16*(3), 201–218. https://doi.org/10.1016/S0951-8339(02)00054-0

Young, I. R. (2006). Directional spectra of hurricane wind waves. *Journal of Geophysical Research*, *111*(C8), C08020. https://doi.org/10.1029/2006JC003540

Yujuan, S., William, P., & Bechara, T. (2018). Simulation of wave-current interactions under hurricane conditions using an unstructured-grid model: Impacts on ocean waves. *Journal of Geophysical Research: Oceans*, *123*(5), 3739–3760. https://doi.org/10.1029/2017JC012939

Zappa, C. J., Banner, M. L., Schultz, H., Corrada-Emmanuel, A., Wolff, L. B., & Yalcin, J. (2008). Retrieval of short ocean wave slope using polarimetric imaging. *Measurement Science and Technology*, *19*(5), 055503. https://doi.org/10.1088/0957-0233/19/5/055503